Journal of Power Sources 252 (2014) 35–42

Contents lists available at ScienceDirect

Journal of Power Sources

journal homepage: www.elsevier.com/locate/jpowsour

Short communication

In-situ visualization of N_2 evolution in operating direct hydrazine hydrate fuel cell by soft X-ray radiography

Tomokazu Sakamoto [a,*], Phengxay Deevanhxay [b], Koichiro Asazawa [a], Shohji Tsushima [b], Shuichiro Hirai [b], Hirohisa Tanaka [a]

[a] R&D Division, Daihatsu Motor Co., Ltd., 3000 Yamanoue, Ryuo, Gamo, Shiga 520-2593, Japan
[b] Department of Mechanical and Control Engineering, Tokyo Institute of Technology, 2-12-1 Ookayama, Meguro-ku, Tokyo 152-8552, Japan

HIGHLIGHTS

- Soft X-ray radiography was performed for in-situ visualization of DHFC.
- The current distribution was confirmed in the anode electrode of 4 cm^2.
- The nitrogen evolution was observed under the rib.

ARTICLE INFO

Article history:
Received 22 September 2013
Received in revised form
24 November 2013
Accepted 28 November 2013
Available online 10 December 2013

Keywords:
In-situ visualization
Soft X-ray radiography
Direct hydrazine hydrate fuel cell
N_2 evolution

ABSTRACT

Soft X-ray radiography technique was firstly applied to operating direct hydrazine hydrate fuel cell (DHFCs) in order to visualize N_2 gas behaviors with high spatial and temporal resolution. Two different cells for in-situ visualization of N_2 gas in the DHFCs in in-plane and through-plane direction were designed and fabricated. The utilization of soft X-ray made the visualization of generated N_2 behavior in the DHFC possible with the spatial resolution of 1.5 μm and the temporal resolution of 2.0 s $frame^{-1}$. In the in-plane visualization, the inhomogeneous N_2 gas distribution, suggesting non-uniform reaction distribution in the anode of DHFC, was observed. In the through-plane visualization, N_2 gas accumulation under the rib of anode and discharge to the channel was clearly observed, which are related with cell performance instability.

1. Introduction

Direct liquid fuel cells, such as the methanol (DMFC), ethanol (DEFC), borohydride (DBFC), formic acid (DFAFC), and hydrazine hydrate (DHFC) systems are attractive candidates for electronics applications, because of their high energy density. Recent developments in DHFC technology have led to full-sized demonstration DHFC indicating their feasibility and promise in future fuel cell vehicles [1–5]. Additionally, DHFC can be operated without any previous metal catalyst, which potentially contributes to cost reduction of the system and compact system. In DHFC, the following electrochemical reactions take place in the anode and the cathode, respectively.

$$\text{Anode}: \quad N_2H_4(\text{liquid}) + 4OH^- \rightarrow N_2(\text{gas}) + 4H_2O + 4e^- \qquad (1)$$

$$\text{Cathode}: \quad O_2 + 2H_2O + 4e^- \rightarrow 4OH^- \qquad (2)$$

$$\text{Overall}: \quad N_2H_4 + O_2 + 2H_2O \rightarrow N_2 + 4H_2O \qquad (3)$$

Thus, hydrazine electrooxidation leads to harmless N_2 and H_2O products, and the theoretical efficiency and theoretical potential (1.62 V) of DHFCs are higher than those of H_2/O_2 PEFCs. Liquid hydrazine evolves N_2 gas bubbles by hydrazine electrochemical oxidation. The generated gases might lead to block the channels and further fuel supply to the catalyst layer is inhibited. Moreover, inhomogeneous current distribution in the anode electrode could have happen due to concentration distribution of

* Corresponding author. Tel.: +81 748 1685; fax: +81 748 57 1064.
E-mail address: tomokazu_sakamoto@dk.daihatsu.co.jp (T. Sakamoto).

0378-7753/$ – see front matter © 2013 Elsevier B.V. All rights reserved.
http://dx.doi.org/10.1016/j.jpowsour.2013.11.108

hydrazine hydrate flowing through the channel between anode inlet and outlet. Therefore, a fundamental understanding of anode N_2 evolution and their effects on the fuel cell performance is essential to improve the DHFCs performance. In previous studies, in-situ visualization of water behavior in proton exchange membrane fuel cell (PEFC) and CO_2 evolution in DMFC using synchrotron X-ray radiography [6–11], neutron radiography [12–19], and soft X-ray radiography [20–26] have been reported. In-situ visualization techniques have been contributed to understand the phenomenon of gas and liquid transport in operating fuel cells. In particular, soft X-ray radiography has been known as a unique laboratory-based method for in-situ diagnostics of liquid water behaviors in operating PEFCs with high spatial resolution of approximately 1 μm.

In this study, we first report in-situ visualization of N_2 evolution and distribution in operating DHFCs by using high resolution soft X-ray radiography and investigate the generated N_2 behaviors with current density variation.

2. Experimental

2.1. Visualization cells for in-situ radiography

In order to observe a wide area of DHFC and prevent the liquid fuel leakage during observation, the cells both in-plane direction and through-plane direction were designed and fabricated by modifying the design of previous visualization cells, which were used for in-situ diagnostic of liquid water by using soft X-ray radiography [20–26]. Fig. 1 shows the cell structure used in this study. To permit the penetration of the soft X-ray through the cells, the carbon current collector was used and the active areas of the in-plane and through-plane cells were 4 cm^2 (2 × 2 cm^2) and 0.1 cm^2 (0.2 × 0.5 cm^2), respectively. The carbon current collector and metal current collector were connected by electrically-conductive adhesive polymer. The serpentine flow-filed separators were used for both anode and cathode in the in-plane cell.

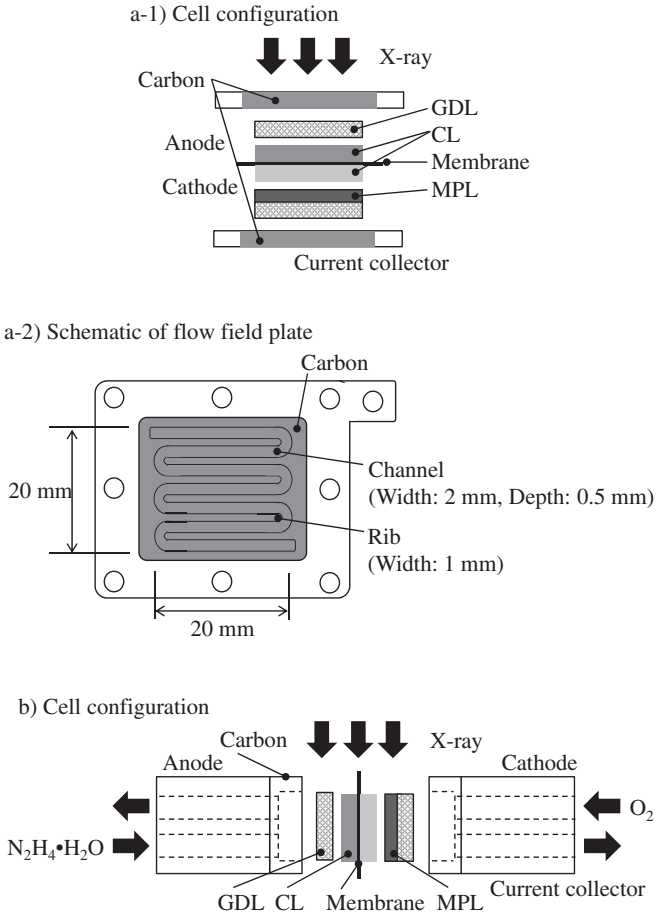

Fig. 1. Schematic view of visualization cell structure. (a) In-plane cell, (b) through-plane cell.

2.2. MEA and operating condition for DHFC

A 100 mg of the catalyst was combined with 0.96 ml of isopropanol, 0.24 ml of THF and 0.2 ml of a 5 wt% anionic ionomer solution (A3, Tokuyama). The ink was then sonicated for 5 min. After sonication, ZrO_2 beads (Diameter = 2.0 mm, Nikkato) were added and the mixture was agitated for 15 min. The prepared ink was directly sprayed onto an anionic electrolyte membrane (A201, Tokuyama) to form the anode electrode on the membrane. Fe-Phen (Phen: phenanthroline) cathode catalyst was formed into an electrode using a similar method to that of the anode. The membrane was then pressed for 5 min at room temperature to bind the catalyst layers to the membrane.

The prepared MEAs, with a square shaped working electrode area of 2 × 2 cm^2 and 0.2 × 0.5 cm^2 for in-plane and through-plane cell, were inserted in each visualization test cell for in-situ radiography. The fuel of 1.0 M KOH + 1.0 M $N_2H_4 \cdot H_2O$ was supplied to the anode at flow rate of 2 ml min^{-1} and 6 ml h^{-1} for in-plane and through-plane cell, respectively. The oxygen was supplied to the cathode at the flow rate of 100 ml min^{-1} and 20 ml min^{-1} for in-plane and through-plane cell, respectively.

2.3. Soft X-ray radiography

The visualization was performed by using a laboratory-base soft X-ray microscope system (Mars Tohken X-ray Inspection Co., Ltd., TUX3110-FC). A tungsten thin-film was used as the target material for generating soft X-rays (W Lα; 8.40 keV, W Lβ; 9.67 keV), and the X-ray tube voltage was set at 17.8 kV. Alignment was performed before observing the fuel cell by using a micro-chart (JIMA RT RC-02), with which a line pitch of 1.5 μm could be discriminated at the cell position. The cell was carefully fixed on a computer controlled four-axis stage that was able to move in the *X*, *Y*, and *Z* directions with a resolution of 1 μm and rotate around the *Z* axis. The stage allowed accurate alignment of the cell with the X-ray beam. The surface of the cell was adjusted to be perpendicular to the X-ray beam. The center of the anode gas diffusion layer (GDL) was aligned with the center of the image reception area of through-plane cell, which was along the beam axis. The images were captured by an imaging system comprised of 1024 × 1024 pixel electron multiplication charge-couple device (EM-CCD) camera with 16-bit depth (Hamamatsu photonics K. K.) and processing computer. All the images were taken at 1 frame per second (fps), and an image with 2 s of integration time was used to calculate the gas distribution. HC-Image (Hamamatsu photonics K. K.) and Image-J (National institute of health) software were used for image processing.

3. Results and discussion

3.1. In-situ visualization using the in-plane cell

In order to investigate the current distribution in anode electrode of DHFC, the in-plane visualization cell (MEA vertical to the X-

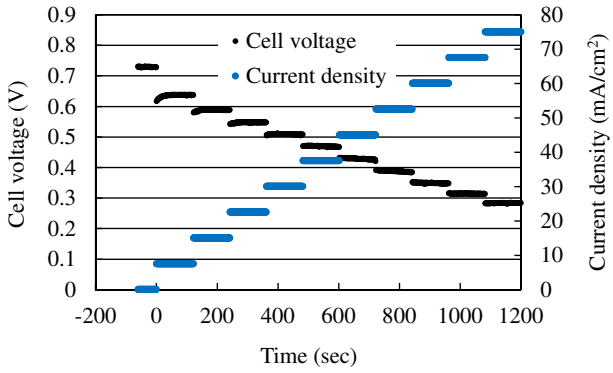

Fig. 2. Current density and cell voltage as a function of time using in-plane cell.

ray beam direction) with an active area of 4 cm^2 (2 × 2 cm^2) was used to visualize the generated gas distribution under the rib and in the channel area within an operating DHFC. Fig. 2 shows the current density and cell voltage as a function of time using in-plane cell. During the in-plane visualization test, the current density of the cell was raised 7.5 mA cm^{-2} stepwise every 120 s by means of programmatic control. The cell performance readily becomes stable after the load is changed as shown in Fig. 2. Fig. 3 shows the low magnification images of the in-plane visualization as a function of time. In this experiment, the temporal resolution of visualization is 2.0 frame per second (fps). All electrode area of 4 cm^2 was visualized using this test cell as shown in Fig. 3. Under the open circuit voltage (OCV) conditions, the cell contains a small amount of gas in the channel due to the gas which is either trapped in the anode catalyst layer including GDL before fuel is supplied into the cell or is generated by chemical decomposition of hydrazine as shown in the following equations (4) and (5).

$$N_2H_4 \rightarrow N_2 + 2H_2 \quad (4)$$

$$3N_2H_4 \rightarrow N_2 + 4NH_3 \quad (5)$$

The volume of generated N_2 due to hydrazine electrooxidation is calculated by equation (1) and Faraday's laws of electrolysis as shown in the following equation (6),

$$V_{N_2} = \frac{It}{zF} V_{STP} \quad (6)$$

where V_{N_2} is the volume of generated N_2, I is the current, t is the total time the constant current was applied (t = 2 s), z is the valence number of ions of the substance (z = 4), F is the Faraday constant (F = 96485 C mol^{-1}), and V_{STP} is the gas volume of 1 mol at standard condition (V_{STP} = 22.4 L). From the above equation (6), V_{N_2} at 7.5 mA cm^{-2} and 37.5 mA cm^{-2} were

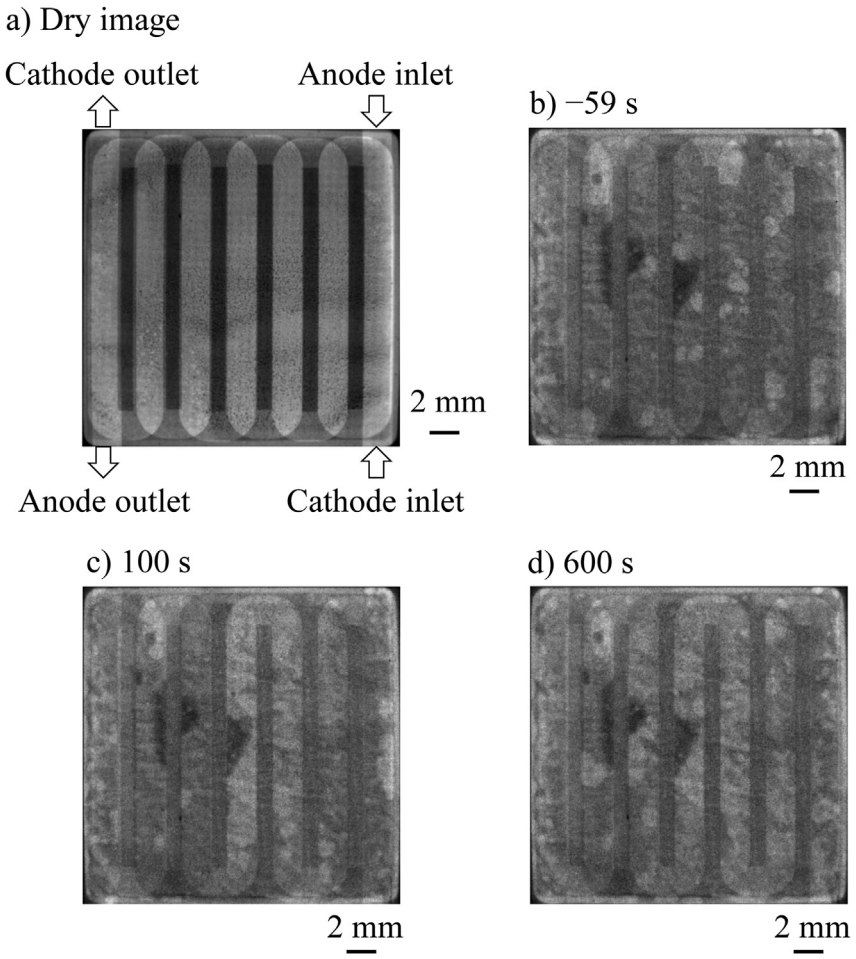

Fig. 3. Low magnification images of the in-plane visualization as a function of time. (a) Dry image, (b) image at −59 s (OCV), (c) image at 100 s (7.5 mA cm^{-2}), (d) image at 600 s (37.5 mA cm^{-2}). The captured time is the time shown in Fig. 2.

calculated 0.0035 ml and 0.0174 ml, respectively. N_2 gas accumulation in the channel was observed with increase in current density as shown in Fig. 3(b) and (c), which was caused by electrochemical oxidation of hydrazine as shown in equation (1). In addition N_2 evolution was observed in large area of anode inlet as shown in Fig. 3, meanwhile N_2 evolution was not identified in the area of anode outlet, suggesting the inhomogeneous current distribution on the anode of DHFC. From these low magnification visualization, it was confirmed that N_2 gas was mainly trapped in the channel, but was flushed away intermittently due to continuous liquid fuel supply.

The current density and cell voltage as a function of time for in-situ radiography of high magnification images using in-plane cell is shown in Fig. 4. Fig. 5 shows the high magnification images under the rib of three different areas as function of time. Area of visualization was approximately 1 × 1 mm^2 in each image. To clarify the behavior of generated gas under the rib, an image processing to extract N_2 gas which caused less soft X-ray attenuation than liquid fuel was carried out as shown in Fig. 5. The gas distribution was determined by image division according to Beer–Lambert law, i.e., by dividing the pixel values of the image during operation with the corresponding pixel values of the image before operation. With increase in current density, N_2 gas generation was clearly observed under the ribs in the inlet and the center as shown in Fig. 5(b) and (c). On the other hand, N_2 gas evolution was not identified in the outlet as shown in Fig. 5(d), suggesting the inhomogeneous current distribution on the anode of DHFC. The result of visualization for N_2 behavior under the rib at high magnification well agreed with the result of visualization at low magnification. The inhomogeneous current distribution on anode of DHFC was caused by N_2 gas accumulation in the channel or catalyst layer. Therefore the quantitative additional research to explain the relationship between inhomogeneous current distribution and N_2 accumulation is required in future research.

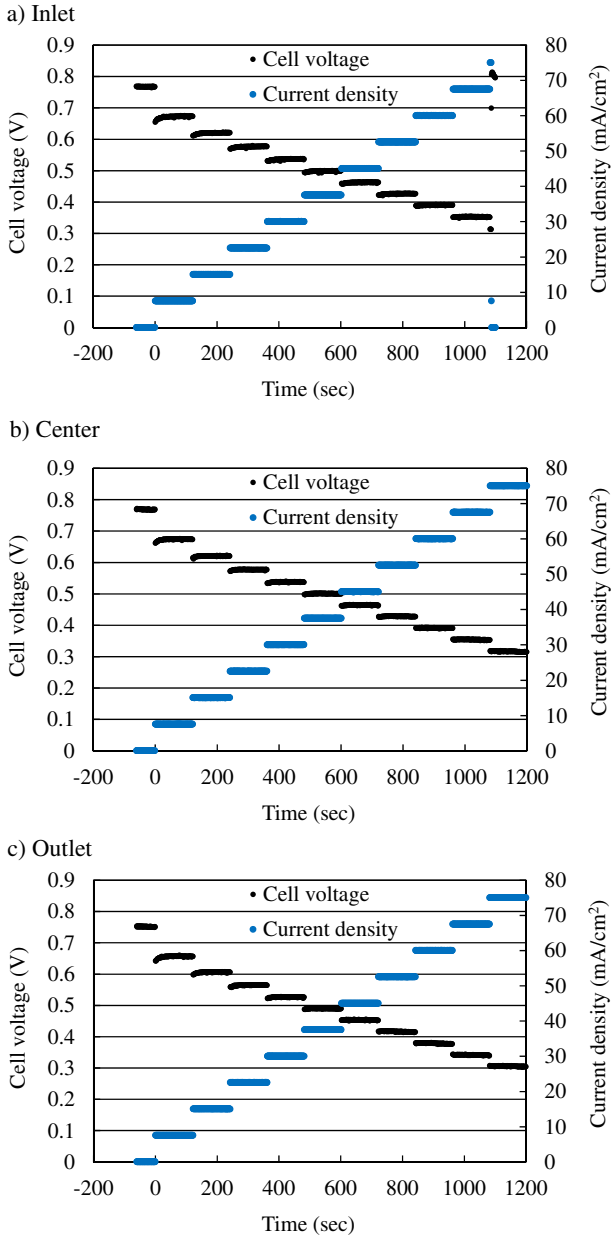

Fig. 4. Current density and cell voltage as a function of time. (a) *I–V* characteristic for in-situ radiography under the rib in the inlet area, (b) center area, (c) outlet area.

3.2. In-situ visualization using the through-plane cell

The through-plane visualization cell with an active area of 0.1 cm^2 (0.5 × 0.2 cm^2) was performed to investigate the effect of N_2 evolution on cell performance of DHFC. Fig. 6 shows the current density and cell voltage as a function of time using through-plane cell. During the through-plane visualization test, the current density of the cell was raised 2 mA cm^{-2} stepwise every 120 s by means of programmatic control. Fig. 7 shows the low magnification images which are divided by image of OCV condition to clarify the behavior of N_2 evolution. The cell performance of through-plane cell was lower and less stable than that of in-plane cell as shown in Fig. 6. In particular, the instability of cell performance was confirmed in the region of high current density. The cell performance decreased when N_2 accumulates in throughout channel, and then cell performance was improved by the discharge of N_2 from the channel. The instability of cell performance using through-plane cell is considered that the generated N_2 by hydrazine oxidation disturbs fuel supply to anode catalyst layer due to a low discharging efficiency of through-plane cell. The current density and cell voltage as a function of time for in-situ radiography of high magnification images using through-plane cell is shown in Fig. 8. Fig. 9 shows the visualization images focused under the rib of anode side using in-situ radiography. After fuel cell startup, N_2 gas evolution under the rib of anode side was clearly observed as shown in Fig. 9(c). Then, some amount of generated N_2 gas was exhausted to the channel from the rib and N_2 gas was accumulated in the channel as observed in Fig. 9(d). At 400 s in Fig. 9(f), N_2 gas under the rib was discharged to the channel, and then fuel distribution into the GDL was observed. From these results, it is clear that the intermittent N_2 gas evolution, accumulation and discharge behaviors affect the cell performances of the DHFC, and thus further investigation can be performed by the soft X-ray radiography technique to capture temporal and spatial variation of N_2 gas in DHFCs.

The contrast of image at cathode side GDL in Fig. 9 was supposed the change of water concentration due to oxygen reduction reaction as shown in the equation (2). The significant change of contrast wasn't observed at OCV condition, however the contrast of image at cathode side GDL was identified with increase in current density as shown in Fig. 9. The water concentration at cathode side is closely related to oxygen reduction reaction on catalyst surface, fuel

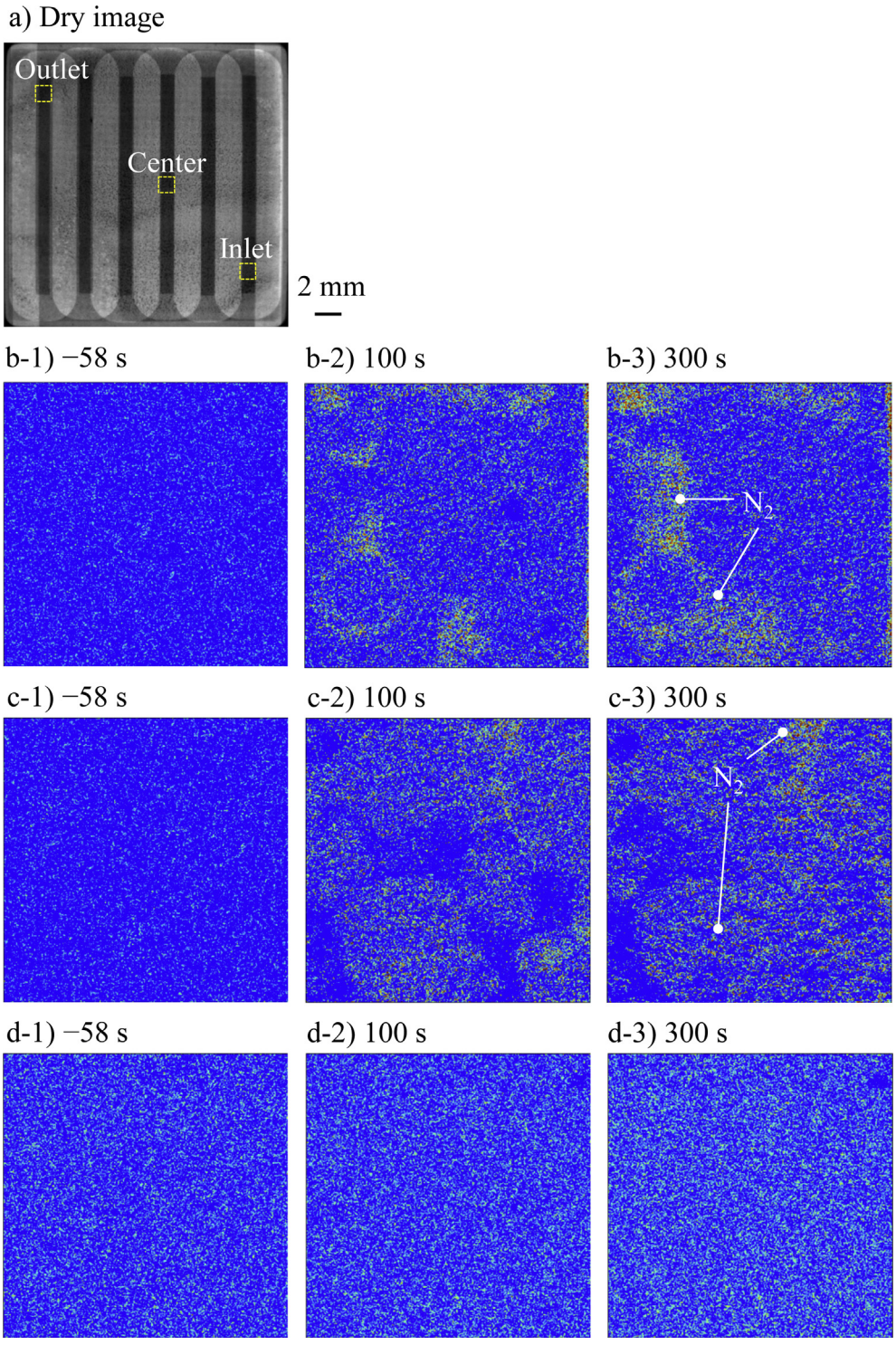

Fig. 5. High magnification images under the rib of in-plane cell as a function of time. (a) Dry image at low magnification; the yellow rectangles indicate the positions at high magnification observation, (b) images at inlet, (c) images at center, (d) images at outlet. The captured times of (b), (c), and (d) are the time shown in Fig. 4(a), (b), and (c), respectively. (For interpretation of the references to color in this figure legend, the reader is referred to the web version of this article.)

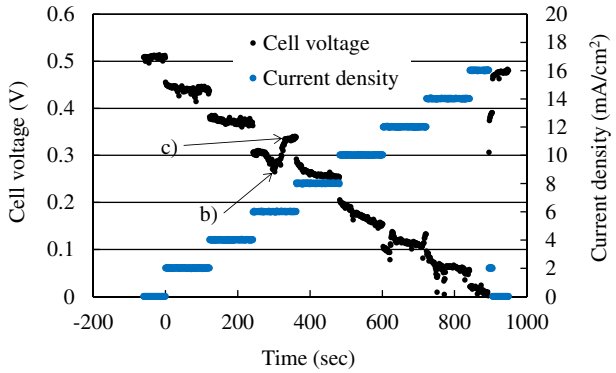

Fig. 6. Current density and cell voltage as a function of time using through-plane cell. The symbols (b) and (c) show the captured time of images (b) and (c) in Fig. 7.

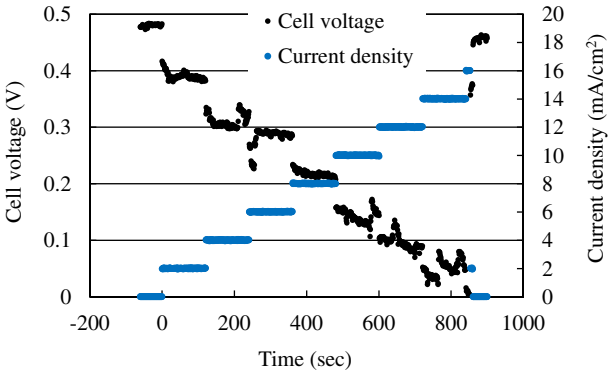

Fig. 8. Current density and cell voltage as a function of time for in-situ radiography of high magnification images using through-plane cell.

penetration from anode side, and humidification condition of air supplied from cathode.

4. Conclusions

Soft X-ray radiography was firstly applied to investigate N_2 evolution, accumulation and discharge behaviors in operating DHFCs. An in-plane cell with 2 × 2 cm^2 active area and a through-plane cell with 0.2 × 0.5 cm^2 active area were developed. In the in-plane visualization, the inhomogeneous N_2 gas distribution, suggesting non-uniform reaction distribution in the anode of DHFC, was observed. In the through-plane visualization, N_2 gas accumulation in the anode rib and discharge to the channel was clearly observed, which are related with cell performance instability.

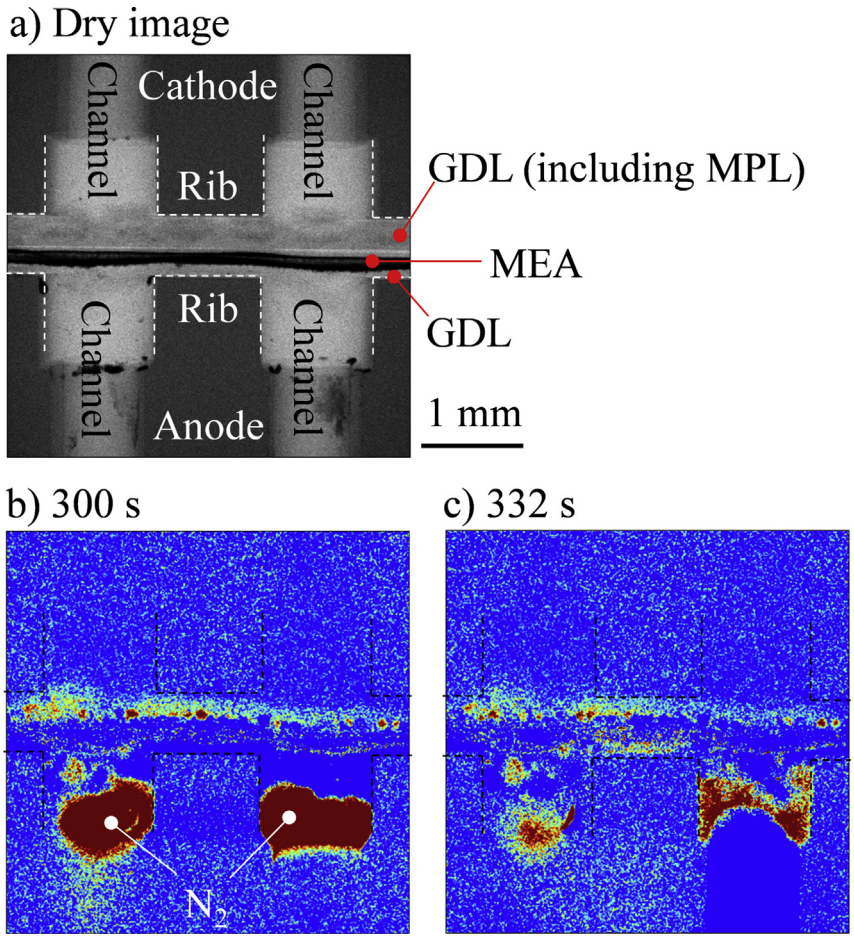

Fig. 7. Low magnification images of the through-plane visualization as a function of time. (a) Dry image, (b) image at 300 s, (c) image at 332 s. The capture time is the time shown in Fig. 6.

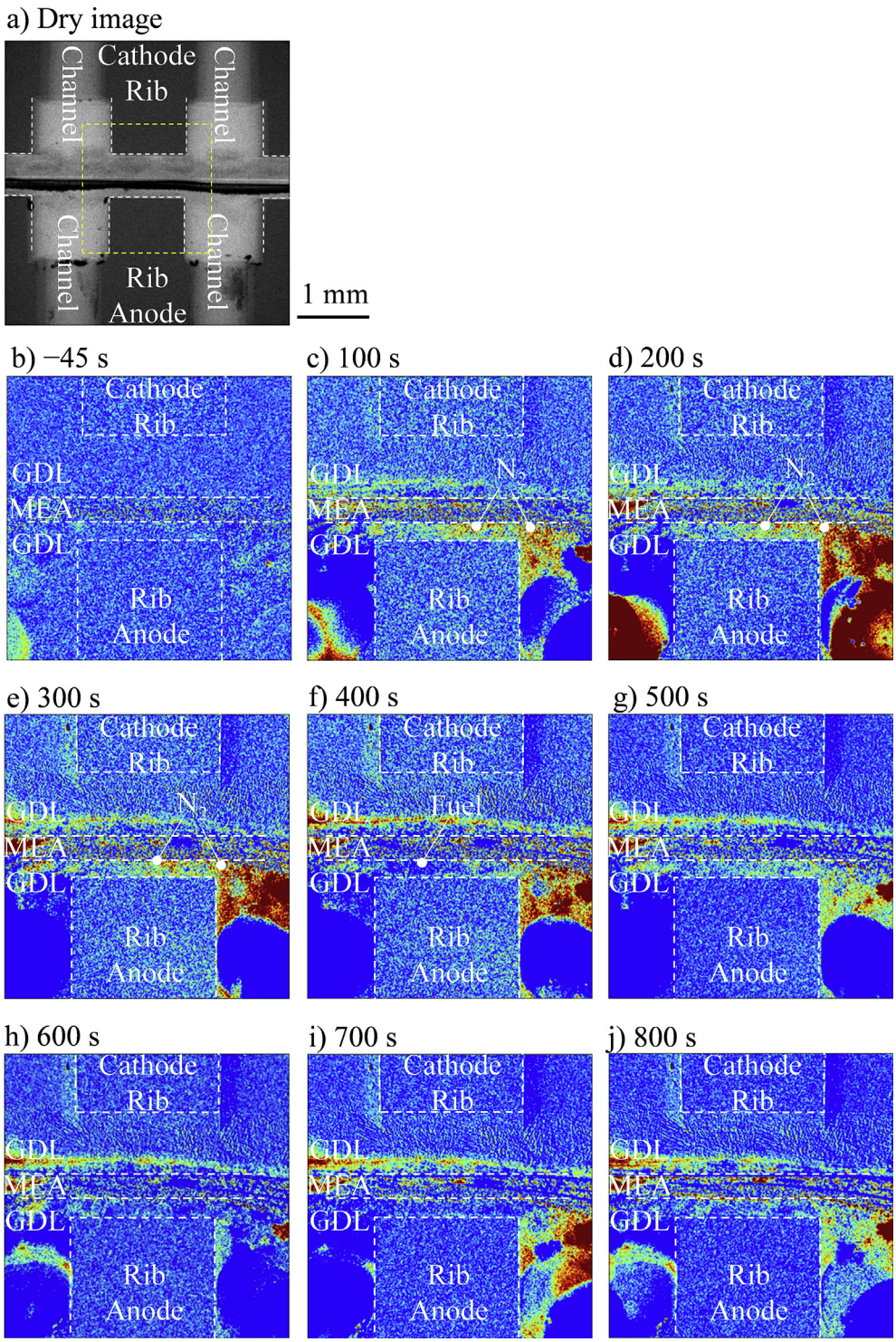

Fig. 9. High magnification images focused under the rib of the anode side of trough-plane cell as a function of time. (a) Dry image at low magnification; the yellow rectangle indicates the positions at high magnification observation, (b–j) visualization images at each time. The captured time is the time shown in Fig. 8. (For interpretation of the references to color in this figure legend, the reader is referred to the web version of this article.)

Acknowledgments

We would like to thank Dr. T. Sasabe (Nagoya Univ.) for his advice on designing of the visualization cell. Soft X-ray visualization technique has been developed by support of the New Energy and Industrial Technology Development Organization (NEDO) of Japan.

References

[1] K. Yamada, K. Yasuda, N. Fujiwara, Z. Siroma, H. Tanaka, Y. Miyazaki, T. Kobayashi, Electrochem. Commun. 5 (2003) 892–896.
[2] K. Asazawa, K. Yamada, A. Oka, M. Taniguchi, T. Kobayashi, Angew. Chem. Int. Ed. 46 (2007) 8024–8027.
[3] W.X. Yin, Z.P. Li, J.K. Zhu, H.Y. Qin, J. Power Sources 182 (2008) 520–523.
[4] A. Serov, C. Kwak, Appl. Catal. B Environ. 98 (2010) 1–9.

[5] T. Sakamoto, K. Asazawa, U. Martinez, B. Halevi, T. Suzuki, S. Arai, D. Matsumura, Y. Nishihata, P. Atanassov, H. Tanaka, J. Power Sources 234 (2013) 252–259.
[6] C. Hartnig, I. Manke, R. Kuhn, S. Kleinau, J. Goebbels, J. Banhart, J. Power Sources 188 (2009) 468–474.
[7] H. Markötter, I. Manke, Ph. Krüger, T. Arlt, J. Haussmann, M. Klages, H. Riesemeier, Ch. Hartnig, J. Scholta, J. Banhart, Electrochem. Commun. 13 (2011) 1001–1004.
[8] J. Haußmann, H. Markötter, R. Alink, A. Bauder, K. Dittmann, I. Manke, J. Scholta, J. Power Sources 239 (2013) 611–622.
[9] H. Markötter, R. Alink, J. Haußmann, K. Dittmann, T. Arlt, F. Wieder, C. Tötzke, M. Klages, C. Reiter, H. Riesemeier, J. Scholta, D. Gerteisen, J. Banhart, I. Manke, Int. J. Hydrogen Energy 37 (2012) 7757–7761.
[10] S.-J. Lee, S.-G. Kim, G.-G. Park, C.-S. Kim, Int. J. Hydrogen Energy 35 (2010) 10457–10463.
[11] C. Hartnig, I. Manke, J. Schloesser, P. Krüger, R. Kuhn, H. Riesemeier, K. Wippermann, J. Banhart, Electrochem. Commun. 11 (2009) 1559–1562.
[12] T.A. Trabold, J.P. Owejan, D.L. Jacobson, M. Arif, P.R. Huffman, Int. J. Heat Mass Transfer 49 (2006) 4712–4720.
[13] J.P. Owejan, T.A. Trabold, D.L. Jacobson, D.R. Baker, D.S. Hussey, M. Arif, Int. J. Heat Mass Transfer 49 (2006) 4721–4731.
[14] M.A. Hickner, N.P. Siegel, K.S. Chen, D.S. Hussey, D.L. Jacobson, M. Arif, J. Electrochem. Soc. 155 (4) (2008) B427–B434.
[15] C. Tötzkea, I. Manke, A. Hilger, G. Choinka, N. Kardjilov, T. Arlt, H. Markötter, A. Schröder, K. Wippermann, D. Stolten, C. Hartnig, P. Krüger, R. Kuhn, J. Banhart, J. Power Sources 196 (2011) 4631–4637.
[16] M. Klages, S. Enz, H. Markötter, I. Manke, N. Kardjilov, J. Scholta, J. Power Sources 239 (2013) 596–603.
[17] J. Zhang, D. Kramer, R. Shimoi, Y. Ono, E. Lehmann, A. Wokaun, K. Shinohara, G.G. Scherer, Electrochim. Acta 51 (2006) 2715–2727.
[18] A. Schröder, K. Wippermann, J. Mergel, W. Lehnert, D. Stolten, T. Sanders, T. Baumhöfer, D.U. Sauer, I. Manke, N. Kardjilov, A. Hilger, J. Schloesser, J. Banhart, C. Hartnig, Electrochem. Commun. 11 (2009) 1606–1609.
[19] A. Schröder, K. Wippermann, T. Arlt, T. Sanders, T. Baumhöfer, N. Kardjilov, J. Mergel, W. Lehnert, D. Stolten, J. Banhart, I. Manke, Int. J. Hydrogen Energy 38 (2013) 2443–2454.
[20] T. Sasabe, S. Tsushima, S. Hirai, Int. J. Hydrogen Energy 35 (2010) 11119–11128.
[21] T. Sasabe, P. Deevanhxay, S. Tsushima, S. Hirai, J. Power Sources 196 (2011) 8197–8206.
[22] T. Sasabe, P. Deevanhxay, S. Tsushima, S. Hirai, Electrochem. Commun. 13 (2011) 638–641.
[23] P. Deevanhxay, T. Sasabe, S. Tsushima, S. Hirai, Int. J. Hydrogen Energy 36 (2011) 10901–10907.
[24] P. Deevanhxay, T. Sasabe, S. Tsushima, S. Hirai, Electrochem. Commun. 22 (2012) 33–36.
[25] P. Deevanhxay, T. Sasabe, S. Tsushima, S. Hirai, Electrochem. Commun. 34 (2013) 239–241.
[26] P. Deevanhxay, T. Sasabe, S. Tsushima, S. Hirai, J. Power Sources 230 (2013) 38–43.